# FUSE: A FAST MULTI-BAND IMAGE FUSION ALGORITHM

*Qi Wei, Nicolas Dobigeon, and Jean-Yves Tourneret*

University of Toulouse, IRIT/INP-ENSEEIHT, 31071 Toulouse cedex 7, France

## ABSTRACT

This paper studies a fast multi-band image fusion algorithm for high-spatial low-spectral resolution and low-spatial high-spectral resolution images. The popular forward model and the conventional Gaussian prior are used to form the posterior of the target image. Maximizing the posterior leads to solving a matrix Sylvester equation. By exploiting the properties of the circulant and decimation matrices associated with the fusion problem, a closed-form solution for the corresponding Sylvester equation is obtained, avoiding any iterative update step. Simulation results show that the proposed algorithm achieves the same performance as existing algorithms with the advantage of significantly decreasing the computational complexity of these algorithms.

***Index Terms***— Multi-band fusion, Hyperspectral images, Sylvester equation, Closed-form solution

## 1. INTRODUCTION

Multi-band images including hyperspectral (HS) and multi-spectral (MS) images have been used successfully in many image processing applications [1, 2]. However, multi-band imaging generally suffers from the limited spatial resolution of the data acquisition devices, mainly due to an unsurpassable tradeoff between spatial and spectral sensitivities [3]. Generally, the linear degradations applied to the observed images with respect to (w.r.t.) the target high-spatial and high-spectral image reduce to spatial and spectral transformations. Thus, the multi-band image fusion problem can be interpreted as restoring a three dimensional data-cube from two degraded data-cubes.

The high-spatial and high-spectral resolution reference image is vectorized band by band to build an $m_\lambda \times n$ matrix $\mathbf{X}$ to better distinguish spectral and spatial degradations, where $m_\lambda$ is the number of spectral bands and $n$ is the number of pixels in each band. Based on this pixel ordering, any linear operation applied to the left (resp. right) side of $\mathbf{X}$ describes a spectral (resp. spatial) degradation.

In this work, we assume that two complementary images of high-spectral or high-spatial resolutions are available to reconstruct the high-spectral and high-spatial resolution image of interest (target image). These images result from linear spectral and spatial degradations of the full resolution image $\mathbf{X}$, according to the well-admitted model

$$\begin{aligned} \mathbf{Y}_{\mathrm{L}} &= \mathbf{L}\mathbf{X} + \mathbf{N}_{\mathrm{L}} \\ \mathbf{Y}_{\mathrm{R}} &= \mathbf{X}\mathbf{B}\mathbf{S} + \mathbf{N}_{\mathrm{R}} \end{aligned} \qquad (1)$$

where $\mathbf{X} \in \mathbb{R}^{m_\lambda \times n}$ is the full resolution target image and $\mathbf{Y}_{\mathrm{L}} \in \mathbb{R}^{n_\lambda \times n}$ and $\mathbf{Y}_{\mathrm{R}} \in \mathbb{R}^{m_\lambda \times m}$ are the observed spectrally and spatially

degraded images. The matrix $\mathbf{L} \in \mathbb{R}^{n_\lambda \times m_\lambda}$ is the spectral degradation, depending on the spectral response of the sensor, which can be *a priori* known or estimated by cross-calibration [4]. The blurring matrix $\mathbf{B} \in \mathbb{R}^{n \times n}$ has the specific property of being a cyclic convolution operator acting on the bands if the spatial blurring is assumed to be space-invariant. The matrix $\mathbf{S} \in \mathbb{R}^{n \times m}$ is a $d = d_r \times d_c$ uniform downsampling operator, which has $m = n/d$ ones on the block diagonal and zeros elsewhere, and such that $\mathbf{S}^T\mathbf{S} = \mathbf{I}_m$. Note that multiplying by $\mathbf{S}^T$ represents zero-interpolation to increase the number of pixels from $m$ to $n$. Finally, the noises $\mathbf{N}_{\mathrm{L}}$ and $\mathbf{N}_{\mathrm{R}}$ are additive terms that include both modeling errors and sensor noises.

This matrix equation (1) has been widely advocated to solve the pansharpening and HS pansharpening problems, which consist of fusing a PAN image with an MS or an HS image [5]. Similarly, most of the techniques developed to fuse MS and HS images also rely on a similar linear model [6, 7]. The problem of fusing high-spectral and high-spatial resolution images can be formulated as estimating the unknown matrix $\mathbf{X}$ from (1). This is a challenging task, mainly due to the large size of $\mathbf{X}$ and to the presence of the downsampling operator $\mathbf{S}$, which prevents any direct use of the Fourier transform to diagonalize the blurring operator $\mathbf{B}$. To overcome this difficulty, several computational strategies have been designed to approximate the Bayesian estimators associated with a Gaussian prior modeling [5, 8]. The method recently proposed in [6] is based on a Markov chain Monte Carlo (MCMC) algorithm which shows good performance but has the major drawback of being computationally expensive. In [9], an alternating direction method of multipliers (ADMM) embedded in a block coordinate descent method (BCD) has been developed to compute the maximum a posterior (MAP) estimator of $\mathbf{X}$, allowing the numerical complexity to be significantly decreased. More fusion methods can also be found in [5].

In this paper, contrary to the algorithms described above, a much more efficient method is proposed to solve explicitly an underlying Sylvester equation (SE) associated with the fusion problem defined in (1), leading to an algorithm referred to as Fast fUsion based on Sylvester Equation (FUSE). The MAP estimator associated with a Gaussian prior similar to [6, 9] can be directly computed thanks to the proposed strategy.

## 2. PROBLEM FORMULATION

Since adjacent HS bands are known to be highly correlated, the HS vectors usually live in a subspace whose dimension is much smaller than the number of bands $m_\lambda$ [10], i.e., $\mathbf{X} = \mathbf{H}\mathbf{U}$ where $\mathbf{H}$ is a full column rank matrix and $\mathbf{U} \in \mathbb{R}^{\tilde{m}_\lambda \times n}$ is the projection of $\mathbf{X}$ onto the subspace spanned by the columns of $\mathbf{H} \in \mathbb{R}^{m_\lambda \times \tilde{m}_\lambda}$.

Considering the statistical properties of the noise matrices $\mathbf{N}_{\mathrm{L}}$ and $\mathbf{N}_{\mathrm{R}}$, it is obvious to formulate the fusion problem linked with the linear model (1) in the least-squares (LS) sense [11] as follow

$$\arg\min_{\mathbf{U}} L(\mathbf{U}) = \arg\min_{\mathbf{U}} d(\mathbf{U}) + \phi(\mathbf{U}) \qquad (2)$$

where

$$d(\mathbf{U}) = \frac{1}{2} \left\| \mathbf{\Lambda}_{\mathrm{R}}^{-\frac{1}{2}} \left( \mathbf{Y}_{\mathrm{R}} - \mathbf{HUBS} \right) \right\|_F^2 + \frac{1}{2} \left\| \mathbf{\Lambda}_{\mathrm{L}}^{-\frac{1}{2}} \left( \mathbf{Y}_{\mathrm{L}} - \mathbf{LHU} \right) \right\|_F^2 \quad (3)$$

is the data term and $\phi(\mathbf{U})$ is the regularizer. In this work, we focus on the Tikhonov (or $\ell_2$) regularization [12], i.e.,

$$\phi(\mathbf{U}) = \frac{1}{2} \left\| \mathbf{\Sigma}^{-\frac{1}{2}} (\mathbf{U} - \boldsymbol{\mu}) \right\|_F^2 \quad (4)$$

where $\boldsymbol{\mu}$ and $\mathbf{\Sigma}$ are fixed and $\mathbf{\Sigma}$ explores the correlations between HS band and controls the distance between $\mathbf{U}$ and $\boldsymbol{\mu}$. In this work, $\boldsymbol{\mu}$ and $\mathbf{\Sigma}$ have been fixed by estimating them from the data directly. However, the optimization w.r.t. the $\ell_2$ regularized objective can appear as a sub-problem of the optimization associated with a more complicated prior, such as total variation (TV) [13], or a hyper-prior in a hierarchical Bayesian framework [7]. This reminds us that the proposed method to solve (2) can be useful when embedded into more sophisticated regularization based models. In this paper, we prove that after exploiting some properties of $\mathbf{B}$ and $\mathbf{S}$, the minimization problem (2) can be solved analytically, without any iterative optimization scheme or Monte Carlo based method. The resulting closed-form solution to the optimization problem (2) is presented in Section 3. Simulation results are presented in Section 4 whereas conclusions are reported in Section 5.

## 3. A CLOSED-FORM SOLUTION FOR MULTI-BAND IMAGE FUSION

### 3.1. Sylvester equation

The matrix $\mathbf{U}$ minimizing $L(\mathbf{U})$ satisfies the relation, $\mathrm{d}L(\mathbf{U})/\mathrm{d}\mathbf{U} = 0$, leading to the following matrix equation

$$\mathbf{H}^H \mathbf{\Lambda}_{\mathrm{R}}^{-1} \mathbf{HUBS} \left( \mathbf{BS} \right)^H + \left( \left( \mathbf{LH} \right)^H \mathbf{\Lambda}_{\mathrm{L}}^{-1} \mathbf{LH} + \mathbf{\Sigma}^{-1} \right) \mathbf{U}$$
$$= \mathbf{H}^H \mathbf{\Lambda}_{\mathrm{R}}^{-1} \mathbf{Y}_{\mathrm{R}} \left( \mathbf{BS} \right)^H + \left( \mathbf{LH} \right)^H \mathbf{\Lambda}_{\mathrm{L}}^{-1} \mathbf{Y}_{\mathrm{L}} + \mathbf{\Sigma}^{-1} \boldsymbol{\mu}. \quad (5)$$

As mentioned in Section 1, the difficulty for solving (5) results from the high dimensionality of $\mathbf{U}$ and the presence of the down-sampling matrix $\mathbf{S}$. In this work, we show that Eq. (5) can be solved analytically with some assumptions summarized below.

**Assumption 1.** *The blurring matrix $\mathbf{B}$ is a block circulant matrix with circulant blocks.*

A consequence of this assumption is that $\mathbf{B}$ can be decomposed as $\mathbf{B} = \mathbf{FDF}^H$ and $\mathbf{B}^H = \mathbf{FD}^* \mathbf{F}^H$, where $\mathbf{F} \in \mathbb{R}^{n \times n}$ is the discrete Fourier transform (DFT) matrix ($\mathbf{FF}^H = \mathbf{F}^H \mathbf{F} = \mathbf{I}_n$), $\mathbf{D} \in \mathbb{R}^{n \times n}$ is a diagonal matrix and $*$ represents the conjugate operator. Note that the blurring matrix $\mathbf{B}$ is assumed to be known. In practice, it can be estimated by cross-calibration [4] or using observed data [13].

**Assumption 2.** *The decimation matrix $\mathbf{S}$ corresponds to downsampling the original signal and its conjugate transpose $\mathbf{S}^H$ interpolates the decimated signal with zeros.*

A decimation matrix satisfies the property $\mathbf{S}^H \mathbf{S} = \mathbf{I}_m$. Moreover, the matrix $\underline{\mathbf{S}} \triangleq \mathbf{SS}^H \in \mathbb{R}^{n \times n}$ is symmetric and idempotent, i.e., $\underline{\mathbf{S}} = \underline{\mathbf{S}}^H$ and $\underline{\mathbf{SS}}^H = \underline{\mathbf{S}}^2 = \underline{\mathbf{S}}$.

Note that the assumptions 1 and 2 for the blurring matrix $\mathbf{B}$ and the decimation matrix $\mathbf{S}$ have been widely used in image processing

applications, such as super-resolution [14], fusion [13], etc. After multiplying (5) on both sides by $\left( \mathbf{H}^H \mathbf{\Lambda}_{\mathrm{R}}^{-1} \mathbf{H} \right)^{-1}$, we obtain[1]

$$\mathbf{C}_1 \mathbf{U} + \mathbf{U} \mathbf{C}_2 = \mathbf{C}_3 \quad (6)$$

where

$$\begin{aligned} \mathbf{C}_1 &= \left( \mathbf{H}^H \mathbf{\Lambda}_{\mathrm{R}}^{-1} \mathbf{H} \right)^{-1} \left( \left( \mathbf{LH} \right)^H \mathbf{\Lambda}_{\mathrm{L}}^{-1} \mathbf{LH} + \mathbf{\Sigma}^{-1} \right) \\ \mathbf{C}_2 &= \mathbf{B}\underline{\mathbf{S}}\mathbf{B}^H \\ \mathbf{C}_3 &= \left( \mathbf{H}^H \mathbf{\Lambda}_{\mathrm{R}}^{-1} \mathbf{H} \right)^{-1} \left( \mathbf{H}^H \mathbf{\Lambda}_{\mathrm{R}}^{-1} \mathbf{Y}_{\mathrm{R}} \left( \mathbf{BS} \right)^H + \left( \mathbf{LH} \right)^H \mathbf{\Lambda}_{\mathrm{L}}^{-1} \mathbf{Y}_{\mathrm{L}} + \mathbf{\Sigma}^{-1} \boldsymbol{\mu} \right). \end{aligned} \quad (7)$$

Eq. (6) is a Sylvester matrix equation [15]. It is well known that an SE has a unique solution if and only if an arbitrary sum of the eigenvalues of $\mathbf{C}_1$ and $\mathbf{C}_2$ is not equal to zero [15]. The matrix $\mathbf{C}_1$ is positive definite as the covariance matrix $\mathbf{\Sigma}^{-1}$ is always positive definite. Thus, the eigenvalues of $\mathbf{C}_1$ are always positive, guaranteeing the existence of the unique solution of (6).

### 3.2. Proposed closed-form solution

Using the decomposition $\mathbf{C}_1 = \mathbf{Q} \mathbf{\Lambda}_C \mathbf{Q}^{-1}$ and multiplying both sides of (6) by $\mathbf{Q}^{-1}$ leads to

$$\mathbf{\Lambda}_C \mathbf{Q}^{-1} \mathbf{U} + \mathbf{Q}^{-1} \mathbf{U} \mathbf{C}_2 = \mathbf{Q}^{-1} \mathbf{C}_3. \quad (8)$$

Right multiplying (8) by $\mathbf{FD}$ on both sides and using the definitions of matrices $\mathbf{C}_2$ and $\mathbf{B}$ yields

$$\mathbf{\Lambda}_C \mathbf{Q}^{-1} \mathbf{UFD} + \mathbf{Q}^{-1} \mathbf{UFD} \left( \mathbf{F}^H \underline{\mathbf{S}} \underline{\mathbf{D}} \right) = \mathbf{Q}^{-1} \mathbf{C}_3 \mathbf{FD} \quad (9)$$

where $\underline{\mathbf{D}} = (\mathbf{D}^*) \mathbf{D}$ is a real diagonal matrix. Note that $\mathbf{UFD} = \mathbf{UBF} \in \mathbb{R}^{\tilde{m}_\lambda \times n}$ can be interpreted as the Fourier transform of the blurred target image, which is a complex matrix. Eq. (9) can be regarded as an SE w.r.t. $\mathbf{Q}^{-1} \mathbf{UFD}$, which has a simpler form compared to (6) as $\mathbf{\Lambda}_C$ is a diagonal matrix.

The next step in our analysis is to simplify the matrix $\mathbf{F}^H \underline{\mathbf{S}} \underline{\mathbf{D}}$ appearing on the left hand side of (9). First, it is important to note that the matrix $\mathbf{F}^H \underline{\mathbf{S}} \underline{\mathbf{D}}$ has a specific structure since all its columns contain the same blocks [16]. Using this property, by multiplying left and right by specific matrices, we will show that we obtain a block matrix whose nonzero blocks are located in its first (block) row (see (12)). More precisely, introduce the following matrix

$$\mathbf{P} = \underbrace{\begin{bmatrix} \mathbf{I}_m & \mathbf{0} & \cdots & \mathbf{0} \\ -\mathbf{I}_m & \mathbf{I}_m & \cdots & \mathbf{0} \\ \vdots & \vdots & \ddots & \vdots \\ -\mathbf{I}_m & \mathbf{0} & \cdots & \mathbf{I}_m \end{bmatrix}}_{d} \quad (10)$$

whose inverse can be easily computed. Right multiplying both sides of (9) by $\mathbf{P}^{-1}$ leads to

$$\mathbf{\Lambda}_C \bar{\mathbf{U}} + \bar{\mathbf{U}} \mathbf{M} = \bar{\mathbf{C}}_3 \quad (11)$$

where $\bar{\mathbf{U}} = \mathbf{Q}^{-1} \mathbf{UFDP}^{-1}$, $\mathbf{M} = \mathbf{P} \left( \mathbf{F}^H \underline{\mathbf{S}} \underline{\mathbf{D}} \right) \mathbf{P}^{-1}$ and $\bar{\mathbf{C}}_3 = \mathbf{Q}^{-1} \mathbf{C}_3 \mathbf{FDP}^{-1}$. Eq. (11) is an SE w.r.t. $\bar{\mathbf{U}}$ whose solution is significantly easier than for (8) because the matrix $\mathbf{M}$ has the following

---

[1]The invertibility of the matrix $\mathbf{H}^H \mathbf{\Lambda}_{\mathrm{R}}^{-1} \mathbf{H}$ is guaranteed since $\mathbf{H}$ has full column rank and $\mathbf{\Lambda}_{\mathrm{R}}$ is positive definite.

simple form

$$\mathbf{M} = \mathbf{P}\left(\mathbf{F}^H \underline{\mathbf{S}} \mathbf{F} \underline{\mathbf{D}}\right)\mathbf{P}^{-1} = \frac{1}{d}\begin{bmatrix} \sum\limits_{i=1}^{d}\underline{\mathbf{D}}_i & \underline{\mathbf{D}}_2 & \cdots & \underline{\mathbf{D}}_d \\ \mathbf{0} & \mathbf{0} & \cdots & \mathbf{0} \\ \vdots & \vdots & \ddots & \vdots \\ \mathbf{0} & \mathbf{0} & \cdots & \mathbf{0} \end{bmatrix} \tag{12}$$

where the matrix $\underline{\mathbf{D}}$ has been partitioned as

$$\underline{\mathbf{D}} = \text{diag}\left[\underline{\mathbf{D}}_1, \underline{\mathbf{D}}_2, \cdots, \underline{\mathbf{D}}_d\right]$$

with $\underline{\mathbf{D}}_i$ an $m \times m$ real diagonal matrix [16].

Finally, using the specific form of $\mathbf{M}$, the solution $\bar{\mathbf{U}}$ of the SE (11) can be computed block-by-block as stated in the following theorem.

**Theorem 1.** *Let $(\bar{\mathbf{C}}_3)_{l,j}$ denotes the $j$th block of the $l$th band of $\bar{\mathbf{C}}_3$ for any $l = 1, \cdots, \widetilde{m}_\lambda$. Then, the solution $\bar{\mathbf{U}}$ of the SE (11) can be decomposed as*

$$\bar{\mathbf{U}} = \begin{bmatrix} \bar{\mathbf{u}}_{1,1} & \bar{\mathbf{u}}_{1,2} & \cdots & \bar{\mathbf{u}}_{1,d} \\ \bar{\mathbf{u}}_{2,1} & \bar{\mathbf{u}}_{2,2} & \cdots & \bar{\mathbf{u}}_{2,d} \\ \vdots & \vdots & \ddots & \vdots \\ \bar{\mathbf{u}}_{\widetilde{m}_\lambda,1} & \bar{\mathbf{u}}_{\widetilde{m}_\lambda,2} & \cdots & \bar{\mathbf{u}}_{\widetilde{m}_\lambda,d} \end{bmatrix} \tag{13}$$

*with*

$$\bar{\mathbf{u}}_{l,j} = \begin{cases} (\bar{\mathbf{C}}_3)_{l,j}\left(\frac{1}{d}\sum\limits_{i=1}^{d}\underline{\mathbf{D}}_i + \lambda_C^l \boldsymbol{I}_n\right)^{-1}, & j = 1, \\ \frac{1}{\lambda_C^l}\left[(\bar{\mathbf{C}}_3)_{l,j} - \frac{1}{d}\bar{\mathbf{u}}_{l,1}\underline{\mathbf{D}}_j\right], & j = 2, \cdots, d. \end{cases} \tag{14}$$

*Proof.* See [16]. □

Note that $\mathbf{u}_{l,j} \in \mathbb{R}^{1 \times m}$ denotes the $j$th block of the $l$th band. Note also that the matrix $\frac{1}{d}\sum\limits_{i=1}^{d}\underline{\mathbf{D}}_i + \lambda_C^l \mathbf{I}_n$ appearing in the expression of $\bar{\mathbf{u}}_{l,1}$ is an $n \times n$ real diagonal matrix whose inversion is trivial. The final estimator of $\mathbf{X}$ is obtained as follows[2]

$$\hat{\mathbf{X}} = \mathbf{H}\mathbf{Q}\bar{\mathbf{U}}\mathbf{P}\mathbf{D}^{-1}\mathbf{F}^H. \tag{15}$$

The resulting FUSE algorithm allowing to compute the estimated image $\hat{\mathbf{X}}$ is summarized in Algorithm 1.

## 4. SIMULATIONS

### 4.1. Simulation Scenario

This section applies the proposed fusion method to HS pansharpening and compares it with state-of-the-art methods investigated in [9]. The reference image considered here as the high-spatial and high-spectral image is a $512 \times 512 \times 160$ HS image acquired in 2010 by the HySpex HS sensor over Villelongue, France ($00°03'$W and $42°57'$N) with $L = 160$ spectral bands ranging from about 408nm to 985nm, a spectral resolution of 3.6nm and a spatial resolution of 0.5m. A composite color image of the scene of interest is shown in Fig. 1 (bottom right).

---

[2]It may happen that the diagonal matrix $\mathbf{D}$ does not have full rank (containing zeros in its diagonal) or is ill-conditioned (having very small numbers in its diagonal), due to a specific blurring kernel. In this case, $\mathbf{D}^{-1}$ can be replaced by $(\mathbf{D} + \tau\mathbf{I}_m)^{-1}$ for regularization purpose, where $\tau$ is a small penalty parameter [17].

---

**Algorithm 1:** Fast Fusion of Multi-band Images (FUSE)

**Input**: $\mathbf{Y}_L, \mathbf{Y}_R, \boldsymbol{\Lambda}_L, \boldsymbol{\Lambda}_R, \mathbf{L}, \mathbf{B}, \mathbf{S}, \mathbf{H}$
    *// Circulant matrix decomposition:*
        $\mathbf{B} = \mathbf{F}\mathbf{D}\mathbf{F}^H$
1  $\mathbf{D} \leftarrow \text{Dec}(\mathbf{B})$;
2  $\underline{\mathbf{D}} = \mathbf{D}^*\mathbf{D}$;
    *// Calculate $\mathbf{C}_1$*
3  $\mathbf{C}_1 \leftarrow \left(\mathbf{H}^H\boldsymbol{\Lambda}_R^{-1}\mathbf{H}\right)^{-1}\left((\mathbf{L}\mathbf{H})^H\boldsymbol{\Lambda}_L^{-1}\mathbf{L}\mathbf{H} + \boldsymbol{\Sigma}^{-1}\right)$;
    *// Decompose of $\mathbf{C}_1$: $\mathbf{C}_1 = \mathbf{Q}\boldsymbol{\Lambda}_C\mathbf{Q}^{-1}$*
4  $(\mathbf{Q}, \boldsymbol{\Lambda}_C) \leftarrow \text{EigDec}(\mathbf{C}_1)$;
    *// Calculate $\bar{\mathbf{C}}_3$*
5  $\bar{\mathbf{C}}_3 \leftarrow \mathbf{Q}^{-1}\left(\mathbf{H}^H\boldsymbol{\Lambda}_R^{-1}\mathbf{H}\right)^{-1}(\mathbf{H}^H\boldsymbol{\Lambda}_R^{-1}\mathbf{Y}_R(\mathbf{B}\mathbf{S})^H$
   $+(\mathbf{L}\mathbf{H})^H\boldsymbol{\Lambda}_L^{-1}\mathbf{Y}_L + \boldsymbol{\Sigma}^{-1}\boldsymbol{\mu})\mathbf{B}\mathbf{F}\mathbf{P}^{-1}$;
    *// Calculate $\bar{\mathbf{U}}$ block by block (d blocks) and band by band ($\widetilde{m}_\lambda$ bands)*
6  **for** $l = 1$ **to** $\widetilde{m}_\lambda$ **do**
      *// Calculate 1st block in lth band*
7      $\bar{\mathbf{u}}_{l,1} = (\bar{\mathbf{C}}_3)_{l,1}\left(\frac{1}{d}\sum\limits_{i=1}^{d}\underline{\mathbf{D}}_i + \lambda_C^l\mathbf{I}_n\right)^{-1}$;
      *// Other blocks in lth band*
8      **for** $j = 2$ **to** $d$ **do**
9        $\bar{\mathbf{u}}_{l,j} = \frac{1}{\lambda_C^l}\left((\bar{\mathbf{C}}_3)_{l,j} - \frac{1}{d}\bar{\mathbf{u}}_{l,1}\underline{\mathbf{D}}_j\right)$;
10    **end**
11 **end**
    **Output**: $\mathbf{X} = \mathbf{H}\mathbf{Q}\bar{\mathbf{U}}\mathbf{P}\mathbf{D}^{-1}\mathbf{F}^H$

---

The reference HS image $\mathbf{X}$ is reconstructed from one HS and one coregistered PAN images. First, the HS image $\mathbf{Y}_R$ has been generated by applying a $5 \times 5$ Gaussian filter and by down-sampling every 4 pixels in both vertical and horizontal directions for each band of $\mathbf{X}$. Second, a PAN image $\mathbf{Y}_L$ has been obtained by averaging the first 81 bands of the HS image. The HS and PAN images are both contaminated by additive centered Gaussian noises. The simulations have been conducted with SNR = 30dB for both HS and PAN images. The observed HS and MS images are shown in the top left and right of Fig. 1 (note that the HS image has been scaled for better visualization). To learn the projection matrix $\mathbf{H}$, a PCA has been conducted. More precisely, the $\widetilde{m}_\lambda = 5$ most discriminant vectors associated with the 5 largest eigenvalues of the sample covariance matrix of the HS image have been computed. These 5 vectors lead to 99.79% of the information contained in the HS image.

The mean $\boldsymbol{\mu}$ of the Gaussian prior was fixed to an interpolated HS image following the strategy proposed in [6]. The covariance matrix of the Gaussian prior is fixed *a priori*. More specifically, the HS image has been interpolated and then blurred and down-sampled to generate the degraded image, referred to as $\bar{\mathbf{Y}}$. The covariance matrix $\boldsymbol{\Sigma}$ was estimated using this degraded image $\bar{\mathbf{Y}}$ and the HS image $\mathbf{Y}_R$ as

$$\tilde{\boldsymbol{\Sigma}} = \frac{(\mathbf{Y}_R - \bar{\mathbf{Y}})(\mathbf{Y}_R - \bar{\mathbf{Y}})^T}{m - 1}.$$

This section compares the performance of the proposed FUSE algorithm with the MAP estimators of [8] and [9].

### 4.2. Fusion performance

To evaluate the quality of fusion methods, five image quality measures are investigated. We propose to use the restored signal-to-noise ratio (RSNR), the averaged spectral angle mapper (SAM), the uni-
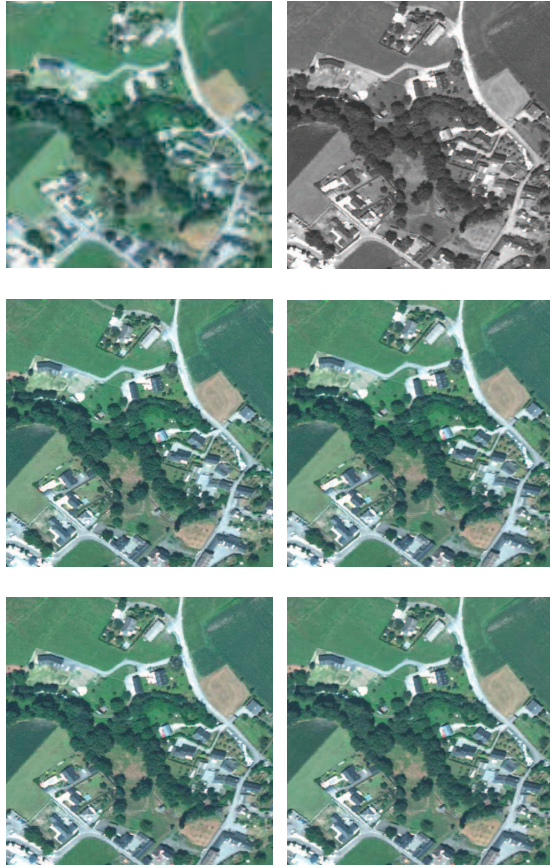
**Fig. 1**. Madonna dataset: (Top left) HS image. (Top right) PAN image. (Middle left) Fusion with method in [8]. (Middle right) Fusion with ADMM in [9]. (Bottom left) Fusion with proposed FUSE. (Bottom right) Reference image.

versal image quality index (UIQI), the relative dimensionless global error in synthesis (ERGAS) and the degree of distortion (DD) as quantitative measures (see [6] for definitions of these performance measures). The larger RSNR and UIQI, the better the fusion. The smaller SAM, ERGAS and DD, the better the fusion.

All algorithms have been implemented using MATLAB R2014A on a computer with Intel(R) Core(TM) i7-2600 CPU@3.40GHz and 8GB RAM. The estimated images obtained with the three algorithms are depicted in Fig. 1 and are visually very similar. More quantitative results are reported in Table 1 and confirm the similar performance of these methods in terms of the various fusion quality measures (RSNR, UIQI, SAM, ERGAS and DD). However, the computational time of the proposed algorithm is reduced by a factor larger than 150 comparing with the result using [9] due to the existence of a closed-form solution for the Sylvester matrix equation.

## 5. CONCLUSION

This paper developed a fast multi-band image fusion method based on an explicit solution of a Sylvester equation. This equation was derived from the maximization of an appropriate posterior distribution associated with the image of interest. Numerical experiments showed that the proposed fast fusion method compares competitively with other state-of-art methods, with the advantage of reducing the computational complexity significantly. Future work will consist of

**Table 1**. Performance of HS Pansharpening methods: RSNR (in dB), UIQI, SAM (in degree), ERGAS, DD (in $10^{-3}$) and time (in second).

| Methods | RSNR | UIQI | SAM | ERGAS | DD | Time |
|---|---|---|---|---|---|---|
| MAP [8] | 18.006 | 0.9566 | 3.801 | 3.508 | 4.687 | 42.08 |
| ADMM [9] | 19.040 | 0.9642 | 3.377 | 3.360 | 4.253 | 159.36 |
| FUSE | 19.212 | 0.9656 | 3.368 | 3.283 | 4.199 | 0.94 |

incorporating spectral unmixing into the multi-band fusion scheme.

## 6. REFERENCES

[1] D. Landgrebe, "Hyperspectral image data analysis," *IEEE Signal Process. Mag.*, vol. 19, no. 1, pp. 17–28, Jan. 2002.

[2] K. Navulur, *Multispectral Image Analysis Using the Object-Oriented Paradigm*, ser. Remote Sensing Applications Series. Boca Raton, FL: CRC Press, 2006.

[3] C.-I. Chang, *Hyperspectral data exploitation: theory and applications*. New York: John Wiley & Sons, 2007.

[4] N. Yokoya, N. Mayumi, and A. Iwasaki, "Cross-calibration for data fusion of EO-1/Hyperion and Terra/ASTER," *IEEE J. Sel. Topics Appl. Earth Observ. Remote Sens.*, vol. 6, no. 2, pp. 419–426, 2013.

[5] L. Loncan, L. B. Almeida, J. M. Bioucas-Dias, X. Briottet, J. Chanussot, N. Dobigeon, S. Fabre, W. Liao, G. Licciardi, M. Simoes, J.-Y. Tourneret, M. Veganzones, G. Vivone, Q. Wei, and N. Yokoya, "Hyperspectral pansharpening: a review," *IEEE Geosci. Remote Sens. Mag.*, to appear.

[6] Q. Wei, N. Dobigeon, and J.-Y. Tourneret, "Bayesian fusion of multiband images," *IEEE J. Sel. Topics Signal Process.*, to appear.

[7] Q. Wei, J. Bioucas-Dias, N. Dobigeon, and J. Tourneret, "Hyperspectral and multispectral image fusion based on a sparse representation," *IEEE Trans. Geosci. Remote Sens.*, vol. 53, no. 7, pp. 3658–3668, Jul. 2015.

[8] R. C. Hardie, M. T. Eismann, and G. L. Wilson, "MAP estimation for hyperspectral image resolution enhancement using an auxiliary sensor," *IEEE Trans. Image Process.*, vol. 13, no. 9, pp. 1174–1184, Sep. 2004.

[9] Q. Wei, N. Dobigeon, and J.-Y. Tourneret, "Bayesian fusion of multispectral and hyperspectral images using a block coordinate descent method," in *Proc. IEEE GRSS Workshop Hyperspectral Image SIgnal Process.: Evolution in Remote Sens. (WHISPERS)*, Tokyo, Japan, Jun. 2015.

[10] J. M. Bioucas-Dias and J. M. Nascimento, "Hyperspectral subspace identification," *IEEE Trans. Geosci. Remote Sens.*, vol. 46, no. 8, pp. 2435–2445, 2008.

[11] C. L. Lawson and R. J. Hanson, *Solving least squares problems*. Englewood Cliffs, NJ: Prentice-hall, 1974, vol. 161.

[12] A. Tikhonov and V. Arsenin, *Solutions of ill-posed problems*, ser. Scripta series in mathematics. Winston, 1977.

[13] M. Simoes, J. Bioucas-Dias, L. Almeida, and J. Chanussot, "A convex formulation for hyperspectral image superresolution via subspace-based regularization," *IEEE Trans. Geosci. Remote Sens.*, vol. 53, no. 6, pp. 3373–3388, Jun. 2015.

[14] M. Elad and A. Feuer, "Restoration of a single superresolution image from several blurred, noisy, and undersampled measured images," *IEEE Trans. Image Process.*, vol. 6, no. 12, pp. 1646–1658, 1997.

[15] R. H. Bartels and G. Stewart, "Solution of the matrix equation AX+ XB= C," *Communications of the ACM*, vol. 15, no. 9, pp. 820–826, 1972.

[16] Q. Wei, N. Dobigeon, and J.-Y. Tourneret, "Fast fusion of multi-band images based on solving a Sylvester equation," *IEEE Trans. Image Process.*, submitted.

[17] R. L. Lagendijk and J. Biemond, *Iterative identification and restoration of images*. New York: Kluwer: Springer Science & Business Media, 1990, vol. 118.